
Article:
Joglekar, A. S., Ridgers, Christopher Paul orcid.org/0000-0002-4078-0887, Kingham, R J et al. (1 more author) (2016) Kinetic modeling of Nernst effect in magnetized hohlraums. Physical Review E. 043206. ISSN 1550-2376

https://doi.org/10.1103/PhysRevE.93.043206

Kinetic modeling of Nernst effect in magnetized hohlraums

A. S. Joglekar,[1,*] C. P. Ridgers,[2] R. J. Kingham,[3] and A. G. R. Thomas[1,†]
[1]*Department of Nuclear Engineering and Radiological Sciences, University of Michigan, Ann Arbor, Michigan 48109, USA*
[2]*York Plasma Institute, Department of Physics, University of York, Heslington, York, YO10 5DD, United Kingdom*
[3]*Blackett Laboratory, Imperial College London, London SW7 2BW, United Kingdom*
(Received 28 August 2015; published 22 April 2016)

We present nanosecond time-scale Vlasov-Fokker-Planck-Maxwell modeling of magnetized plasma transport and dynamics in a hohlraum with an applied external magnetic field, under conditions similar to recent experiments. Self-consistent modeling of the kinetic electron momentum equation allows for a complete treatment of the heat flow equation and Ohm's law, including Nernst advection of magnetic fields. In addition to showing the prevalence of nonlocal behavior, we demonstrate that effects such as anomalous heat flow are induced by inverse bremsstrahlung heating. We show magnetic field amplification up to a factor of 3 from Nernst compression into the hohlraum wall. The magnetic field is also expelled towards the hohlraum axis due to Nernst advection faster than frozen-in flux would suggest. Nonlocality contributes to the heat flow towards the hohlraum axis and results in an augmented Nernst advection mechanism that is included self-consistently through kinetic modeling.

DOI: 10.1103/PhysRevE.93.043206

There has been recent interest in the role of applied magnetic fields in high-energy-density plasmas [1–3] for inertial fusion energy applications [4]. The Magneto-Inertial Fusion Electric Discharge System has been developed to provide steady-state magnetic fields for long time scales relative to the experiments. An experiment at the Omega Laser Facility with a 7.5-T external axial magnetic field imposed on an Omega-scale hohlraum measured a rise in observed temperature along the hohlraum axis [5] and modeling showed that external fields can guide hot electrons from laser-plasma interactions [6] through the hohlraum, rather than the capsule [7].

From Ohm's law, it has been shown that electron heat transport advects such magnetic fields through the Nernst effect [8–14] in addition to well-known processes such as frozen-in flow and resistive diffusion. Dimensionless numbers comparing the ratio of the magnitudes of the Nernst term to the bulk plasma flow term $R_N \gg 1$ [10] and the Hall term $H_N \gg 1$ [13] suggest that Nernst convection should be the dominant mechanism for magnetic field transport in a hohlraum. Such a hot and semi-collisional environment is, however, rich in nonequilibrium effects that may complicate the magnetic field dynamics.

Laser heating of the plasma results in steep temperature gradients, typically $O(3\,\mathrm{keV}/50\,\mu\mathrm{m})$. The collisional mean free path of a 3-keV electron is $O(10\,\mu\mathrm{m})$, depending on the plasma density. Since $\lambda_{\mathrm{mfp}}/L < 100$, nonlocality can be expected to be important [15]. The steep temperature gradients caused by intense laser heating in a hohlraum have been shown to result in nonlocal heat flow [16,17]. Careful consideration of the electron population with $2v_{\mathrm{th}} < v < 4v_{\mathrm{th}}$ is required as these carry most of the heat. Additionally, inverse-bremsstrahlung heating of a plasma [18,19] leads to not only deviations from Braginskii transport [20], but also new transport terms [21,22]. Both nonlocality and laser heating result in modifications to the distribution function and nonequilibrium behavior that result in a breakdown of the classical transport approximations. In order to avoid those approximations, a *kinetic approach* is necessary. This allows for modeling of magnetic field dynamics through a self-consistent and generalized Ohm law derived without distribution function approximations.

Using a Vlasov-Fokker-Planck-Maxwell formulation, we show simulations of magnetized, two-dimensional (2D) hohlraum-scale plasma including ray tracing of an Omega-like laser configuration over a nanosecond time scale. Therefore, this simulation includes self-consistent treatment of the fully kinetic Ohm law and nonlocal effects in heat flow. The hohlraum is considered without a fuel capsule but with a gas fill throughout. Note that radiation transport and laser-plasma interactions are neglected in these calculations. While these may modify the magnitude of the electron temperature near the high-density plasma, the conclusions presented here primarily arise as a result of the nonlocal dynamics prevalent within the low-density optically thin gas fill where the radiation effects will be negligible [23]. With the use of IMPACTA [24,25], we studied the effect of nonequilibrium electron kinetics on thermal energetic and magnetic field dynamics of a Omega-scale hohlraum with an externally imposed 7.5 T magnetic field. We found that significant proportions of the total heat flow are nonlocal. Additionally, the presence of inverse-bremsstrahlung heating resulted in anomalous heat flow towards the overdense plasma of the hohlraum wall. Therefore, the diffusive heat flow from the laser-heated regions is not an adequate description of the thermal energetics. Heat flow from the laser heating moves the externally imposed magnetic field through Nernst advection. To examine the effects of Nernst advection in relation to plasma bulk flow, we show modeling without an electron contribution to the transport of the magnetic field in Ohm's law for comparison.

We find that magnetic field transport due to Nernst flow results in significantly faster field cavitation than via frozen-in flux. The field cavitation occurs due to nonlocal heat flow towards the hohlraum axis. Retention of the distribution function allows for accurate modeling of the magnetic field pileup because the local approximation of the Nernst velocity underestimates the true velocity by a factor of 2. Nernst flow

*Present address: Particle-In-Cell and Kinetic Simulation Center, University of California, Los Angeles, Los Angeles, California 90095, USA; archis@ucla.edu
†agrt@umich.edu

into the overdense region causes a flux pileup at the walls and results in magnetic field amplification by a factor of 3.

The Vlasov-Fokker-Planck equation for electrons given by

$$\left[\frac{\partial}{\partial t}+\mathbf{v}\cdot\frac{\partial}{\partial \mathbf{x}}+\frac{e}{m_e}(\mathbf{E}+\mathbf{v}\times\mathbf{B})\cdot\frac{\partial}{\partial \mathbf{v}}\right]f(\mathbf{v},\mathbf{r},t)$$
$$=-\frac{\partial}{\partial \mathbf{v}}\cdot\{f(\mathbf{v},\mathbf{r},t)\langle\Delta\mathbf{v}\rangle\}+\frac{1}{2}\frac{\partial}{\partial \mathbf{v}}\frac{\partial}{\partial \mathbf{v}}:\{f(\mathbf{v},\mathbf{r},t)\langle\Delta\mathbf{v}\Delta\mathbf{v}\rangle\} \quad (1)$$

is coupled with Ampere's and Faraday's laws and a hydrodynamic ion fluid model to describe the plasma. The code we use, IMPACTA [24,25], uses a Cartesian tensor expansion, with the distribution function expanded as $f(t,\mathbf{r},\mathbf{v})=f_0+\mathbf{f}_1\cdot\hat{\mathbf{v}}+\underline{\underline{\mathbf{f}}}_2:\hat{\mathbf{v}}\hat{\mathbf{v}}+\cdots$, where $\hat{\mathbf{v}}(\theta,\phi)$ is a unit velocity vector. This expansion can be truncated in collisional plasma, as collisions smooth out angular variations resulting in a nearly isotropic distribution, represented by f_0. Higher orders are successively smaller perturbations $f_0\gg\mathbf{f}_1\gg\underline{\underline{\mathbf{f}}}_2$, etc. In the classical limit that f_0 is a Maxwell-Boltzmann velocity distribution, IMPACTA has been shown to agree with Braginskii's transport equations [24]. These simulations, however, are collisional enough such that $\underline{\underline{\mathbf{f}}}_2$ is neglected to an error $O(\lambda_{\rm mfp}/L)^2$.

A two-dimensional slice of a hohlraum is modeled in the x-y plane where the y axis represents the longitudinal axis of the hohlraum and the fuel pellet would sit at the origin. The hohlraum walls are represented by dense high-Z plasma located at approximately $x=\pm800$ μm and the gas fill is represented by low-Z plasma, with the overall Z distribution described by $Z(x,y)=59.25+19.75\tanh(\frac{x-750}{40})$. The electron number density is described by $n_e(x,y)=[2.98+2.93\tanh(\frac{x-750}{40})]\times10^{22}$ cm^{-3}. The initial uniform temperature is $k_BT_{e0}=160$ eV. The initial uniform magnetic field is $\mathbf{B}_0(\hat{y})=7.5$ T and $\ln\Lambda_{ei}=5.4$. To convert from the normalized units, $n_{e0}=5\times10^{20}$ cm^{-3} and $v_{\rm th0}/c=0.025$ are used. The laser parameters resemble those of Ref. [5]. The ray tracing package tracks the three beam cones that enter at 21°, 42°, and 59° from the axis, to their respective refraction points.

The rays and initial heating profile are shown in Fig. 1(a). Figure 1(b) shows the temperature profile after 300 ps of laser heating. Figure 1(c) shows the cavitation and amplification in the in-plane magnetic field profile caused by intense laser heating. The Nernst velocity, shown in Fig. 1(d), is directed towards the hohlraum axis in the low-density gas fill and into the hohlraum wall in the Au plasma. In the rest of this paper, we show that Nernst flow is primarily responsible for the magnetic field profile shown in Fig. 1(c).

Inverse-bremsstrahlung heating of plasma results in a super-Gaussian electron distribution [18], which modifies the transport coefficients [21,26,27] and introduces new terms including an anomalous heat flux up a pressure gradient $\mathbf{q}_n$, represented by the last term in

$$\mathbf{q}_e=-\frac{T_e}{e}\underline{\underline{\psi}}'\cdot\mathbf{j}-(\underline{\underline{\kappa}}+n_e\underline{\underline{\phi}})\cdot\nabla T_e-T_e\underline{\underline{\phi}}\cdot\nabla n_e, \quad (2)$$

where ψ, ϕ, and κ are transport coefficients. These are functions of the local magnetic field, current, and temperature gradients and density gradients, as described in Ref. [21]. Equation 2 recovers the calculation from Ref. [26] in the limit where f_0 is a Maxwell-Boltzmann velocity distribution. Further, $\mathbf{q}_n$ increases as $m>2$ increases, where m is the power of the super-Gaussian distribution function defined by $f_{\rm SG}(v)=C(m)n_e/v_{\rm th}^3\exp[-(v/\alpha_e v_{\rm th})^m]$, where $\alpha_e=[3\Gamma(3/m)/2\Gamma(5/m)]^{1/2}$ and $C(m)=m/4\pi\alpha_e^3\Gamma(3/m)$.

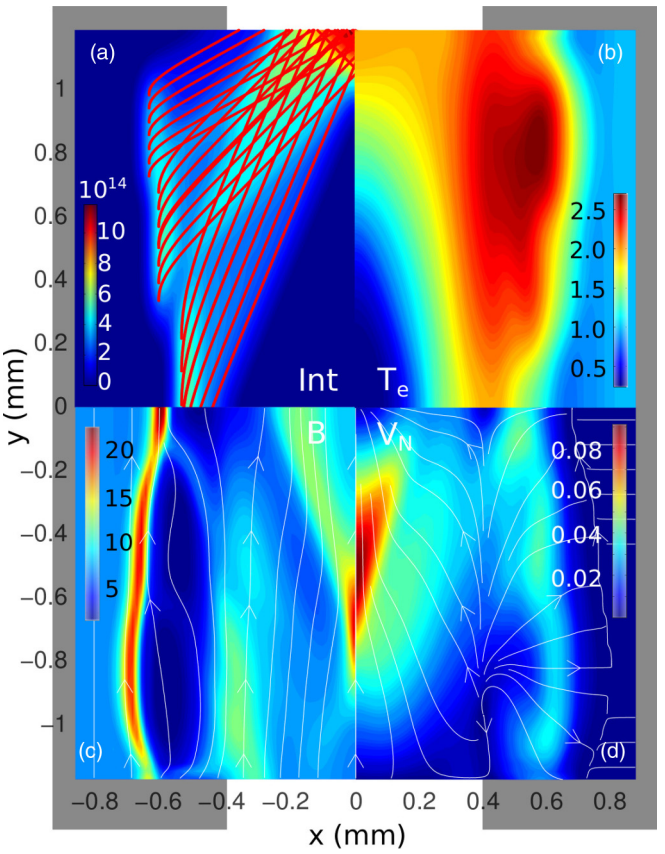

FIG. 1. (a) Ray tracing profile overlaid onto laser intensity profile (W/cm^2) at $t=0$, (b) electron plasma temperature (keV), (c) externally applied magnetic field (T), and (d) Nernst velocity $v_N/v_{\rm th0}$ at $t=250$ ps.

In these simulations, by finding the best fit of a super-Gaussian distribution to the low-velocity part of f_0, m reaches a maximum of 3.1 near the centers of the laser-heated regions, but varies spatially and temporally, thus requiring the preservation of the distribution function at each point throughout the simulation for accurate calculation of the heat flow. Using theory detailed in Refs. [21,27], the heat flow can be modified in hydrodynamics codes to include this effect. However, the distribution is not precisely a super-Gaussian function [28] due to other effects such as nonlocality, magnetic fields, and collisions and this fix remains an approximation.

A postprocessed calculation of the anomalous heat flow shows that there is heat flow towards the hohlraum wall due to the $\phi\nabla P_e$ term and this approximately results in a 10% correction to the diffusive heat flow, i.e., $\kappa\nabla T_e$. A majority of the disagreement between the heat flow from the code and the postprocessed heat flow from all three terms from Eq. (2) stems from the strongly nonlocal heat flow that is prevalent in the hohlraum. Figure 2(b) shows a 2D profile of a metric for quantifying the discrepancy between the two heat flows, described by the relative difference between the super-Gaussian approximation and the exact heat fluxes $1-q_{\text{Eq. (2)}}/q_{\rm code}$.

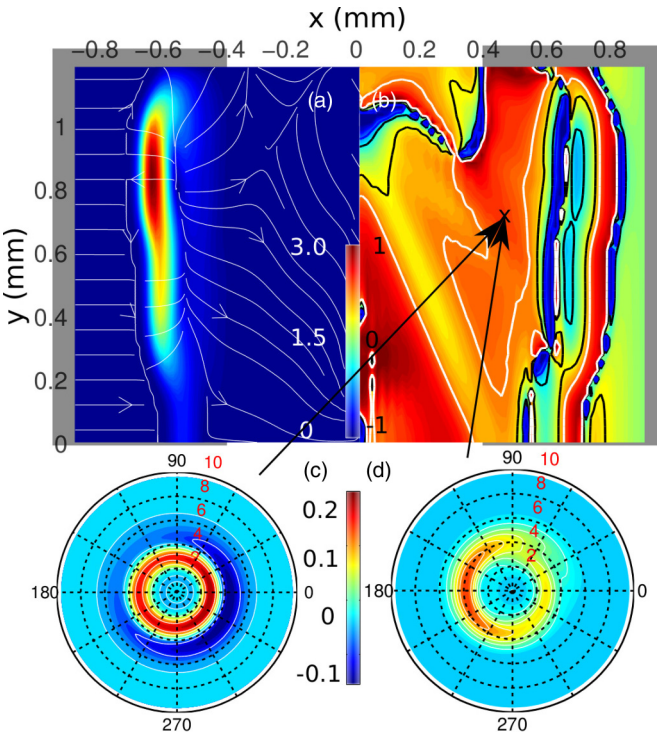

FIG. 2. (a) Heat flow $m_e n_{e0} v_{th0}^3$, (b) $1 - q_{\text{Eq. (2)}}/q_{\text{code}}$, (c) $v^5(f_{\text{code}} - f_{\text{MB}})$, and (d) $v^5(f_{\text{code}} - f_{\text{SG}})$ at $x = 0.4$ mm, $y = -0.6$ mm, $m = 2.625$, and $t = 100$ ps.

The regions within black contours have ±25% agreement between the two heat flows. The white contours correspond to regions of high nonlocality where the super-Gaussian transport calculation is an underapproximation, while the blue contours correspond to regions where the heat flow is significantly overcalculated. Heat flow from regions near the temperature hot spots, ±50 μm, is overestimated by the super-Gaussian calculation, while the heat flow farther away from the hot spots, ±200 μm, is underestimated, as expected from the existence of nonlocality. The regions of relative agreement are ±50–200 μm from the hot spots.

Consideration of the in-plane electron distribution function $f(\theta, v) = f_0 + f_{1x}\hat{v}_x + f_{1y}\hat{v}_y$ can show the significance of inverse-bremsstrahlung heating and nonlocality. Since $\mathbf{q} \propto \int v^5 f(\theta, v)\hat{\mathbf{v}}(\theta, \phi) dv \sin\theta \, d\theta \, d\phi$, the important contributions to the heat flow may be best illustrated by the function $v^5 f(\theta, v)$. Figures 2(c) and 2(d) show the difference between the calculated distribution $v^5 f$ and a Maxwell-Boltzmann $v^5 f_{\text{MB}}$ [Fig. 2(c)] and a super-Gaussian distribution with the best fit to m [Fig. 2(d)], both with $T_e(x = 0.4, y = -0.6)$. Figure 2(c) shows that $f > f_{\text{MB}}$ in the region $2 < v_{\text{th}} < 4$ and $f < f_{\text{MB}}$ in the region $4 < v_{\text{th}} < 6$, which is characteristic of inverse-bremsstrahlung heating. Calculating the heat flow contribution difference between the real distribution and the best-fit super-Gaussian distribution ($m \approx 2.625$ in this case) shows that the inverse-bremsstrahlung model does not replicate the distribution function fully due to anisotropy from the flow and nonlocality. The enhanced tail and shifted center in the 180° direction is characteristic of the (nonlocal) heat flow down the density gradient, while the colder return flow is a result of the features in the 0° direction.

As shown in Ref. [9], the Nernst velocity is given by

$$\mathbf{v}_N = \frac{\langle \mathbf{v} v^3 \rangle}{2\langle v^3 \rangle} + \frac{\mathbf{j}}{e n_e} \tag{3}$$

$$\approx \frac{\overleftrightarrow{\kappa} \cdot \nabla T_e}{5/2 P_e}. \tag{4}$$

It can be shown for this geometry that B_y has no field generation terms from the curl of Ohm's law and therefore can be transported through the $(\mathbf{v}_N + \mathbf{C}) \times \mathbf{B}$ term in addition to resistive diffusion. Over 0.5 ns, the simulation shows that there is magnetic field cavitation resulting in a flux pileup on the hohlraum axis and compression at the hohlraum wall due to the energy deposition from the laser. The pileup of magnetic flux results in a 25-T magnetic field, more than 3 times the strength of the initial 7.5-T field.

In order to determine the effect of Nernst advection on the magnetic field evolution, simulations with and without the $\mathbf{B} \times \mathbf{f}_1$ term in the $\mathbf{f}_1$ equation were compared. This term is responsible for the interaction of kinetic electrons with the magnetic field and therefore is responsible for the Nernst and Hall terms in Ohm's law as well as the Righi-Leduc effect in the heat flow equation. Simulations agree with the previous determination that $\mathbf{j} \ll \mathbf{v}_N$ because $H_N \ll 1$ and the Hall effect can be neglected. The magnetic field after 50 ps without and with full Ohm's law treatment is shown in Figs. 3(a) and 3(b),

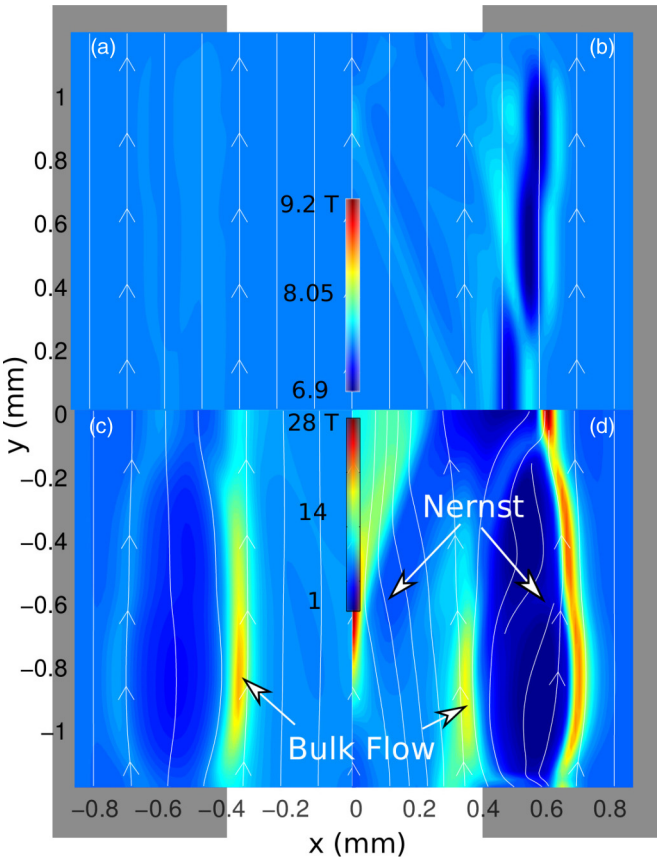

FIG. 3. Magnetic field **B** (T) after 50 ps with (a) only plasma bulk flow and (b) the full Ohm law. Magnetic field **B** after 400 ps with (c) only plasma bulk flow and (d) the full Ohm law.

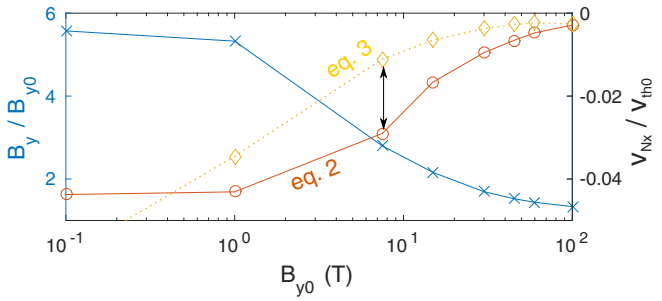

FIG. 4. Magnetic field at the hohlraum axis decreases as applied field strength is increased because the Nernst effect is mitigated, preventing the magnetic field from accumulating near the hohlraum axis ($t = 300$ ps). The discrepancy between the approximated and exact Nernst velocities also decreases.

respectively. The field has been expelled from the laser-heated region in both cases but the magnitudes differ. It is not evident in Fig. 3(a) since the field is only modified by a few percent by the plasma bulk flow. Thermal energy transport results in a more noticeable change immediately over 50 ps.

An estimate of the time scale for plasma bulk flow to transport frozen-in magnetic fields to the hohlraum axis is given by $\frac{r_H}{C_s} \approx \frac{r_H}{\sqrt{k_B T_e / M_i}} \sim 2$ ns. Figure 3(d) shows that including the Nernst effect results in magnetic field cavitation on a faster time scale than can be expected due to field advection only through bulk plasma flow in Fig. 3(c). Given a 7.5-T initial field strength, the magnetic field on the axis grows to 30 T within 0.5 ns. Figure 3(d) also shows that the magnetic flux pileup in the hohlraum wall occurs due to the Nernst effect, increasing to a strength of nearly 25 T towards the hohlraum wall.

We ran a series of simulations with varying initial applied field B_{y0} to understand how field strength affects the hohlraum dynamics. Figure 4 shows the results of these simulations, which suggest that the limiting behavior as the magnetic field is increased is given by

$$\lim_{B_{y0}\to\infty} B_{y\,\mathrm{axis}}/B_{y0} = 1. \tag{5}$$

The maximum value of v_N in the domain of magnetic field advection towards the axis (-0.5 mm $< x < 0.5$ mm) is chosen. This trend can be explained by the observed reduction in the Nernst velocity towards the hohlraum axis as the magnetization increases (also shown in Fig. 4), which quenches magnetic field transport. These $v_N(\omega\tau)$ curves are in line with other predictions [9,13,21] that $v_N \propto 1/\omega\tau$ for $\omega\tau \gg 1$. Figure 4 also shows that the exact Nernst velocity from Eq. (3) is consistently, and up to 2 times, larger than what the local approximation from Eq. (4) would predict for T_e, n_e, and **B** profiles at 300 ps. This discrepancy decreases at higher field strengths due to magnetic field induced localization of the heat flow carrying electrons.

The degree of magnetic flux pileup in the hohlraum wall, however, is not affected strongly by the increase in magnetic field strength because $\omega\tau \sim n_e^{-1}$. The magnitude of maximum field strength in the wall ranges from $2 < B_y/B_{y0} < 3$ for $1 < B_{y0} < 100$ T.

The IMPACTA modeling is in agreement with the HYDRA modeling performed in [5] with respect to the hydrodynamic motion of the plasma only. In that sense, the hydrodynamic ion model that is coupled to the electron transport model in IMPACTA agrees. While it is not possible to compare the modeling in the two works directly, the IMPACTA modeling seeks to highlight the fact that magnetic field transport in [5] is inadequate because it does not include Nernst convection.

We have shown Vlasov-Fokker-Planck modeling of external magnetic fields of 1–100 T imposed upon an Omega-scale hohlraum. Magnetic flux pileup increases the magnetic field magnitude by a factor of 3 for a 7.5-T magnetic field. Additionally, the heat flow is responsible for magnetic field cavitation on a faster time scale than that from the bulk flow of the plasma. Not only is the heat flow strongly nonlocal, it also has distinct signatures of inverse bremsstrahlung heating. The ability to preserve distribution function information through use of a kinetic code allows us to model the heat flow accurately. A full Vlasov-Fokker-Planck-Maxwell treatment of the system enables accurate modeling of the magnetic field dynamics. We have shown that Nernst flow is the dominant mechanism for magnetic field transport and is responsible for the increase in field strength, up to 100 T for an initial 100-T field, in the wall as well as cavitation of the magnetic field towards the hohlraum axis. The field cavitation is mitigated at higher field strengths. Furthermore, the Nernst velocity is up to 2 times larger in self-consistent nonlocal calculations than would be predicted by diffusive transport.

These findings suggest that attempting the same calculation with diffusive transport would result in significantly different **B** and T_e evolution. Accurate modeling of these quantities has implications for laser-plasma interactions [5,6] and hot electron propagation [7] in the gas fill and understanding hot spots on the dense plasma that generate x rays. The kinetic electron transport and **B** field physics presented here could affect details of x-ray drive if incorporated into full-scale radiation-hydrodynamics modeling (including reduced phenomenological laser-plasma interaction models) of indirect drive with an externally applied B field.

The authors would like to thank A. Hazi, J. Moody, and D. Strozzi of LLNL and A. Sefkow of Sandia for useful discussions regarding related work at NIF and Omega. The modeling was performed using computational resources and services provided by Advanced Research Computing at the University of Michigan, Ann Arbor. This research was supported by the DOE through Grant No. DE-SC0010621.

[1] P. Y. Chang, G. Fiksel, M. Hohenberger, J. P. Knauer, R. Betti, F. J. Marshall, D. D. Meyerhofer, F. H. Séguin, and R. D. Petrasso, Phys. Rev. Lett. **107**, 035006 (2011).

[2] M. Hohenberger, P. Y. Chang, G. Fiksel, J. P. Knauer, R. Betti, F. J. Marshall, D. D. Meyerhofer, F. H. Séguin, and R. D. Petrasso, Phys. Plasmas **19**, 056306 (2012).

[3] G. Fiksel, W. Fox, A. Bhattacharjee, D. H. Barnak, P. Y. Chang, K. Germaschewski, S. X. Hu, and P. M. Nilson, Phys. Rev. Lett. **113**, 105003 (2014).
[4] J. D. Lindl, P. Amendt, R. L. Berger, S. G. Glendinning, S. H. Glenzer, S. W. Haan, R. L. Kauffman, O. L. Landen, and L. J. Suter, Phys. Plasmas **11**, 339 (2004).
[5] D. S. Montgomery, B. J. Albright, D. H. Barnak, P. Y. Chang, J. R. Davies, G. Fiksel, D. H. Froula, J. L. Kline, M. J. Macdonald, A. B. Sefkow, L. Yin, and R. Betti, Phys. Plasmas **22**, 010703 (2015).
[6] S. P. Regan, N. B. Meezan, L. J. Suter, D. J. Strozzi, W. L. Kruer, D. Meeker, S. H. Glenzer, W. Seka, C. Stoeckl, V. Y. Glebov, T. C. Sangster, D. D. Meyerhofer, R. L. McCrory, E. A. Williams, O. S. Jones, D. A. Callahan, M. D. Rosen, O. L. Landen, C. Sorce, and B. J. MacGowan, Phys. Plasmas **17**, 020703 (2010).
[7] D. J. Strozzi, L. J. Perkins, M. M. Marinak, D. J. Larson, J. M. Koning, and B. G. Logan, J. Plasma Phys. **81**, 475810603 (2015).
[8] A. Nishiguchi, T. Yabe, M. G. Haines, M. Psimopoulos, and H. Takewaki, Phys. Rev. Lett. **53**, 262 (1984).
[9] M. G. Haines, Plasma Phys. Controlled Fusion **28**, 1705 (2000).
[10] C. P. Ridgers, R. J. Kingham, and A. G. R. Thomas, Phys. Rev. Lett. **100**, 075003 (2008).
[11] L. Willingale, A. G. R. Thomas, P. M. Nilson, M. C. Kaluza, S. Bandyopadhyay, A. E. Dangor, R. G. Evans, P. Fernandes, M. G. Haines, C. Kamperidis, R. J. Kingham, S. Minardi, M. Notley, C. P. Ridgers, W. Rozmus, M. Sherlock, M. Tatarakis, M. S. Wei, Z. Najmudin, and K. Krushelnick, Phys. Rev. Lett. **105**, 095001 (2010).
[12] C. K. Li, F. Séguin, J. Frenje, N. Sinenian, M. Rosenberg, M.-E. Manuel, H. Rinderknecht, A. Zylstra, R. Petrasso, P. Amendt, O. Landen, A. Mackinnon, R. Town, S. Wilks, R. Betti, D. Meyerhofer, J. Soures, J. Hund, J. Kilkenny, and A. Nikroo, Nucl. Fusion **53**, 073022 (2013).
[13] A. S. Joglekar, A. G. R. Thomas, W. Fox, and A. Bhattacharjee, Phys. Rev. Lett. **112**, 105004 (2014).
[14] L. Lancia *et al.*, Phys. Rev. Lett. **113**, 235001 (2014).
[15] D. R. Gray, J. D. Kilkenny, M. S. White, P. Blyth, and D. Hull, Phys. Rev. Lett. **39**, 1270 (1977).
[16] G. Gregori, S. H. Glenzer, J. Knight, C. Niemann, D. Price, D. H. Froula, M. J. Edwards, R. P. J. Town, A. Brantov, W. Rozmus, and V. Y. Bychenkov, Phys. Rev. Lett. **92**, 205006 (2004).
[17] J. Hawreliak, D. M. Chambers, S. H. Glenzer, A. Gouveia, R. J. Kingham, R. S. Marjoribanks, P. A. Pinto, O. Renner, P. Soundhauss, S. Topping, E. Wolfrum, P. E. Young, and J. S. Wark, J. Phys. B **37**, 1541 (2004).
[18] A. B. Langdon, Phys. Rev. Lett. **44**, 575 (1980).
[19] J. M. Liu, J. S. De Groot, J. P. Matte, T. W. Johnston, and R. P. Drake, Phys. Rev. Lett. **72**, 2717 (1994).
[20] S. I. Braginskii, Rev. Plasma Phys. **1**, 205 (1965).
[21] C. P. Ridgers, A. G. R. Thomas, R. J. Kingham, and A. P. L. Robinson, Phys. Plasmas **15**, 092311 (2008).
[22] W. Y. Huo and Q. Zeng, Phys. Plasmas **22**, 094503 (2015).
[23] J. Morton (private communication).
[24] R. J. Kingham and A. R. Bell, J. Comput. Phys. **194**, 1 (2004).
[25] A. G. R. Thomas, R. J. Kingham, and C. P. Ridgers, New J. Phys. **11**, 033001 (2009).
[26] E. M. Epperlein and M. G. Haines, Phys. Fluids **29**, 1029 (1986).
[27] J. J. Bissell, C. P. Ridgers, and R. J. Kingham, New J. Phys. **15**, 025017 (2013).
[28] E. Fourkal, V. Y. Bychenkov, W. Rozmus, R. Sydora, C. Kirkby, C. E. Capjack, S. H. Glenzer, and H. A. Baldis, Phys. Plasmas **8**, 550 (2001).